

# Neural-ANOVA: Model Decomposition for Interpretable Machine Learning

Steffen Limmer, Steffen Udluft, Clemens Otte

<sup>1</sup>Siemens AG, Technology, Munich, Germany  
steffen.limmer@siemens.com

## Abstract

The analysis of variance (ANOVA) decomposition offers a systematic method to understand the interaction effects that contribute to a specific decision output. In this paper we introduce *Neural-ANOVA*, an approach to decompose neural networks into glassbox models using the ANOVA decomposition. Our approach formulates a learning problem, which enables rapid and closed-form evaluation of integrals over subspaces that appear in the calculation of the ANOVA decomposition. Finally, we conduct numerical experiments to illustrate the advantages of enhanced interpretability and model validation by a decomposition of the learned interaction effects.

## Introduction

Deploying machine learning models for regression or control tasks in industrial settings often entails meeting specific certification requirements. These requirements can vary depending on the application domain and the criticality of the task, and may ultimately determine whether a particular machine learning model can be used. Ensuring compliance may involve testing the model against a series of cases curated by domain experts or conducting comprehensive evaluations under adverse operating conditions to confirm that the model accurately captures expected interaction effects.

In addition to certification, machine learning models intended for industrial use must often satisfy robustness and explainability criteria. A challenge in this context may be handling missing data, which can arise from various issues such as sensor failures, preprocessing errors, connectivity problems, calibration faults, or data corruption during storage. Addressing missing or corrupted data is particularly problematic for industrial machine learning models operating at short cycle times (e.g., less than 1 ms). In such cases, advanced imputation techniques can be too slow, and simpler methods like mean or median imputation may not provide the necessary performance.

Another critical challenge involves ensuring transparency and providing explanations for the decision-making processes of AI systems. Techniques collectively referred to as Explainable AI (XAI) aim to mitigate the "black box" nature of models like neural networks by elucidating the dependencies that lead to specific decisions. Achieving XAI is especially crucial for control systems or neural process models, where comprehending the decisions is essential.

The functional analysis of variance (ANOVA) decomposition addresses these challenges by separating interaction effects in order to gain deeper insights into the effects and dependencies between input variables and output variable, owing to its ability to decompose complex relationships into lower-order effects. The ANOVA decomposition has proven valuable in various industrial domains such as modeling of batteries (Adachi et al. 2023) and fluid flows (Yang et al. 2012).

A primary challenge in computing the ANOVA decomposition arises from the need to evaluate higher-dimensional integrals over subspaces of the input domain. Often, this problem is addressed by numerical approximation techniques or by restricting the approximation space to random-forests (Hutter, Hoos, and Leyton-Brown 2014) or spline functions (Potts and Schmischke 2021), for which efficient integration techniques are available. However, each of the latter introduces an error due to approximation, model bias or admits limited expressivity for a given task.

In this study, we introduce a novel method for applying the ANOVA decomposition based on standard neural networks, resulting in models that are more interpretable and suitable for industrial machine learning applications. We refer to these models as *Neural-ANOVA* models. Our key contributions are as follows:

1. We introduce a novel learning formulation that enables rapid and closed-form evaluation of integrals over subspaces appearing in the ANOVA decomposition of neural networks.
2. We demonstrate that Neural-ANOVA models include Generalized Additive Models (GAMs) as a special case, showing comparable performance across various datasets. Our proposed framework supports diverse activation functions and layer sizes, utilizing only nested automatic differentiation and the sum of evaluations.
3. Through extensive evaluations on various regression tasks, encompassing both synthetic test functions and real-world industrial datasets, we show that Neural-ANOVA models can outperform GAMs by incorporating appropriate higher-order interactions.

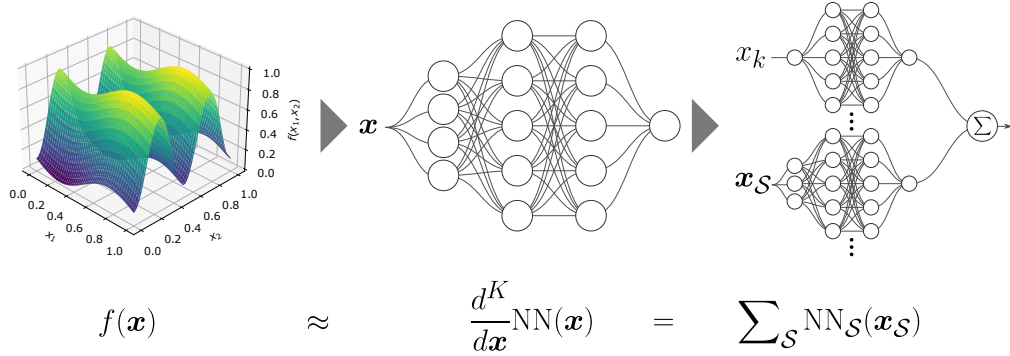


Figure 1: Neural-ANOVA decomposition. The original data is approximated by the mixed derivative of a neural network (NN). A closed-form ANOVA decomposition is obtained by decomposing the trained NN into lower-dimensional subnetworks  $\text{NN}_{\mathcal{S}}(\mathbf{x}_{\mathcal{S}})$ . These subnetworks are derived through closed-form evaluation of integrals over subspaces.

## Related Work

### Generalized and Neural Additive Models

Generalized Additive Models (GAMs) (Hastie 2017) are a powerful and versatile approach for machine learning problems. They extend Generalized Linear Models (GLMs) by incorporating non-linear relationships between features and the target variable through flexible shape functions. GAMs are applicable to both regression and classification tasks and have been successfully used in various domains such as healthcare or finance (Hegselmann et al. 2020; Berg 2007).

A key advantage of GAMs is their interpretability, which stems from their structure of univariate interactions

$$f(\mathbf{x}) = f_0 + \sum_{i=1}^K f_k(x_k), \quad (1)$$

or including also bivariate interactions

$$f(\mathbf{x}) = f_0 + \sum_{k=1}^K f_k(x_k) + \sum_{k=1}^K \sum_{l < k}^K f_{kl}(x_k, x_l). \quad (2)$$

The influence of each feature on the prediction can be comprehensively understood by visualizing its corresponding shape functions. Various methods are available for fitting Generalized Additive Models (GAMs). One traditional method is *backfitting* (Breiman and Friedman 1985), which iteratively updates the components of the model by sequentially refitting them. Another common approach involves spline-based regression (Wahba 1990). More recently, several machine learning approaches have been proposed that leverage conventional gradient descent algorithms. Notably, *Neural Additive Models* (NAMs) (Agarwal et al. 2021), use neural networks to represent the shape functions and are trained using standard stochastic gradient descent techniques. However, the authors note some considerations when using NAMs. Computationally, the optimization process can be challenging and demands careful selection of hyperparameters and application of regularization techniques. Furthermore, choosing the appropriate representation for shape functions is crucial to avoid overfitting or underfitting the data, necessitating careful consideration and experimentation.

### ANOVA Decomposition

The functional ANOVA decomposition (Hoeffding and Robbins 1948; Sobol 2001; Hooker 2004) is a statistical technique for the dimension-wise decomposition of a square-integrable function  $f : \mathcal{X}^K \rightarrow \mathbb{R}$  into a sum of lower-dimensional functions  $f_{\mathcal{S}}$  according to

$$f(\mathbf{x}) = \sum_{\mathcal{S} \subseteq \mathcal{K}} f_{\mathcal{S}}(\mathbf{x}_{\mathcal{S}}). \quad (3)$$

Here, each function  $f_{\mathcal{S}}$  only depends on a subset of variables indexed by the set  $\mathcal{S} \subseteq \mathcal{K}$  and the sum ranges over all  $2^K$  subsets of  $\mathcal{K} := \{1, \dots, K\}$ .

A specific construction and algorithm was proposed in (Hooker 2004; Kuo et al. 2010), necessitating the computation of several multidimensional integrals of the form

$$f_{\mathcal{S}}(\mathbf{x}_{\mathcal{S}}) = \int_{\mathcal{X}^{K-|\mathcal{S}|}} f(\mathbf{x}) d\mathbf{x}_{\mathcal{K} \setminus \mathcal{S}} - \sum_{\mathcal{U} \subsetneq \mathcal{S}} f_{\mathcal{U}}(\mathbf{x}_{\mathcal{U}}), \quad (4)$$

where first term represents an integral over a subset of variables, while the second term subtracts all proper subsets in a manner similar to backfitting. The resulting computational algorithm is detailed in Alg. 1. Using this approach, one can demonstrate that all terms  $f_{\mathcal{S}}$  are orthogonal with respect to the inner product  $\langle f, g \rangle = \int f(\mathbf{x}) \cdot g(\mathbf{x}) d\mathbf{x}$ . Additionally, this construction exhibits the favorable property that the functional variance

$$\sigma^2 = \int f^2(\mathbf{x}) d\mathbf{x} - \left( \int f d\mathbf{x} \right)^2 \quad (5)$$

can be decomposed into the sum of individual component variances

$$\sigma^2 = \sum_{\mathcal{S}} \sigma_{\mathcal{S}}^2 = \sum_{\mathcal{S}} \int f_{\mathcal{S}}^2(\mathbf{x}_{\mathcal{S}}) d\mathbf{x}_{\mathcal{S}}. \quad (6)$$

Furthermore, it can be shown that the decomposition is *minimal* in the sense that no unnecessary terms are being introduced in the decomposition. To illustrate this minimality, consider a function  $f(x_1, x_2) = 2x_1$  where the ANOVA decomposition ensures that no unfavorable non-minimal terms

such as  $f(x_1, x_2) = x_1 - x_2 + (x_1 + x_2)$  are introduced (Kuo et al. 2010).

The minimality property also allows to define meaningful dimensionalities for a function. For instance, one such dimension can be described as the *superposition dimension* of a function, defined as

$$f(\mathbf{x}) = \sum_{|S| \leq d_s} f_S(\mathbf{x}_S), \quad (7)$$

where the variance decomposes according to

$$\sum_{|S| \leq d_s} \sigma_S^2 = \sigma^2. \quad (8)$$

In other words, if a function  $f$  has an effective superposition dimension  $d_s$ , it implies that interactions involve no more than  $d_s$  variables. Furthermore, if a function has an effective superposition dimension of 1, it indicates the existence of an ideal regressor in the form of a Generalized Additive Model (GAM).

The *truncation dimension* is another meaningful quantity that is said to hold with dimension  $d_t$  if there exists a set of truncation variables  $\mathcal{T}$  with  $|\mathcal{K} \setminus \mathcal{T}| = d_t$  such that

$$f(\mathbf{x}) = \sum_{S \subseteq \mathcal{K} \setminus \mathcal{T}} f_S(\mathbf{x}_S), \quad (9)$$

with

$$\sum_{S \subseteq \mathcal{K} \setminus \mathcal{T}} \sigma_S^2 = \sigma^2. \quad (10)$$

Using the truncation dimension, we can identify sets of relevant and irrelevant variables. Additionally, we can use the truncated sum (9) to approximate the function if the variables in the set  $\mathcal{T}$  are unavailable, e.g., due to sensor corruption or processing errors. However, in such scenarios, we should not expect a perfect approximation, meaning the equalities in (9, 10) will not hold.

Various methods for numerically approximating the ANOVA decomposition have been introduced in the literature. These methods include approaches based on random forests (Hutter, Hoos, and Leyton-Brown 2014) and orthonormal systems utilizing polynomial or Fourier basis functions (Potts and Schmischke 2021). Each approach incorporates different model-specific approximation techniques for evaluating the integral (4). The effectiveness of these approximation schemes can be constrained by the expressivity of the chosen model or the maximum order of interactions that can be efficiently included in the numerical approximation process.

Moreover, integrating a numerical approximation scheme into the training loop of a machine learning model is challenging. This difficulty arises from the need to balance the number of required evaluations with the acceptable level of approximation error. For example, (Owen 2023) report needing approximately ten thousand function evaluations to achieve an acceptable approximation error in a five-dimensional setting using quasi-Monte Carlo integration.

## Automatic Integration

Analytical integration is generally considered more challenging than differentiation. Various strategies for exact integration include variable substitution, integration by parts,

**Input:**  $f \in \mathcal{L}_2([0, 1]^K)$

**Output:** functions  $\{f_S\}_{S \subseteq \mathcal{K}}$ , variances  $\{\sigma_S\}_{S \subseteq \mathcal{K}}$

$f_\emptyset := \int_{\mathcal{X}^K} f(\mathbf{x}) d\mathbf{x}; \sigma_\emptyset := 0;$

**for**  $S \subseteq \mathcal{K}, S \neq \emptyset$  **do**

$f_S(\mathbf{x}_S) := \int_{\mathcal{X}^{K-|S|}} f(\mathbf{x}) d\mathbf{x}_{\mathcal{K} \setminus S} - \sum_{U \subsetneq S} f_U(\mathbf{x}_U);$   
     $\sigma_S^2 := \int_{\mathcal{X}^{|S|}} f_S^2(\mathbf{x}_S) d\mathbf{x}_S;$

**end**

$\sigma^2 := \int_{\mathcal{X}^K} f^2(\mathbf{x}) d\mathbf{x} - \left(\int_{\mathcal{X}^K} f(\mathbf{x}) d\mathbf{x}\right)^2 \equiv \sum_{S \subseteq \mathcal{K}} \sigma_S^2;$

**Algorithm 1:** ANOVA decomposition of  $f$  proposed by (Kuo et al. 2010).

and partial fractions. Closed-form solutions for general antiderivatives, i.e., indefinite integrals, are limited to a small class of functions and often involve complex algorithms such as the Risch algorithm (Risch 1969). Numerical integration methods, including Riemann sums, quadratures, and Monte Carlo methods (Owen 2023), are commonly used in practice. These methods typically require a tradeoff between the number of samples and accuracy.

Neural networks, being universal function approximators, can also be utilized for analytical integration within the framework of *automatic integration* (Lindell, Martel, and Wetzstein 2021). This technique involves training a neural network to approximate the antiderivative so that integrals can be obtained by evaluating the trained network at the boundary points of the integration domain. The approach relies on taking derivatives of the neural network, applied repeatedly to all input coordinates and subsequently used to fit the training data. Using this method enables the computation of any definite  $D$ -dimensional integral using  $2^D$  evaluations of a neural network. It has inspired a range of applications, such as neural radiance fields (Gao et al. 2022), tomography (Rückert et al. 2022), pathloss prediction (Limmer, Alba, and Michailow 2023) and neural point processes (Zhou and Yu 2024).

## Neural ANOVA Decomposition

In this section, we present our main contribution, which provides a rapid and closed-form evaluation of integrals over subspaces of the type given by (4) in the ANOVA decomposition, utilizing neural networks.

### Bivariate Example

We begin by demonstrating the fundamental process of automatic integration using a sample bivariate function,  $f(x_1, x_2)$ , to emphasize the differences in the training approach. Conventional neural network training typically involves minimizing a loss function of the form

$$r(\boldsymbol{\theta}) = \sum_i \phi\left(f(x_1^{(i)}, x_2^{(i)}) - \text{NN}(\boldsymbol{\theta}, x_1^{(i)}, x_2^{(i)})\right), \quad (11)$$

where  $\phi$  denotes an appropriate loss function, such as the absolute error or squared error.

In the proposed method, we aim to fit samples of a given function  $f(x_1, x_2)$  while simultaneously calculating

integrals over the input domain. The work (Lindell, Martel, and Wetzstein 2021) suggests training a neural network  $\text{NN}(\boldsymbol{\theta}, x_1, x_2)$  by differentiating the network with respect to all its input coordinates, specifically evaluating its mixed partial derivative. The training process involves minimizing a loss function defined as

$$r(\boldsymbol{\theta}) = \sum_i \phi \left( f(x_1^{(i)}, x_2^{(i)}) - \frac{d}{dx_1} \frac{d}{dx_2} \text{NN}(\boldsymbol{\theta}, x_1^{(i)}, x_2^{(i)}) \right). \quad (12)$$

To ensure computational efficiency, the term  $\frac{d}{dx_1} \frac{d}{dx_2} \text{NN}(\boldsymbol{\theta}, x_1, x_2)$  can be compiled just-in-time and evaluated during the training process using standard techniques in automatic differentiation.

After successful optimization, the optimized neural network parameters, denoted as  $\boldsymbol{\theta}^*$ , are obtained. Integrals can then be computed by evaluating the neural network at the corner points of the integration domain,  $[l_1, u_1] \times [l_2, u_2]$  according to

$$\int_{l_1}^{u_1} \int_{l_2}^{u_2} f(x_1, x_2) dx_1 dx_2 \quad (13)$$

$$= \text{NN}(\boldsymbol{\theta}, l_1, l_2) - \text{NN}(\boldsymbol{\theta}, u_1, l_2) - \text{NN}(\boldsymbol{\theta}, l_1, u_2) + \text{NN}(\boldsymbol{\theta}, u_1, u_2) \quad (14)$$

$$:= \text{NN}(\boldsymbol{\theta}, x_1, x_2) \Big|_{x_1, x_2 \in (l_1, u_1) \times (l_2, u_2)}. \quad (15)$$

### High-dimensional Generalization

Next, we present the generalization of automatic integration to calculate higher-dimensional integrals that appear in Alg. 1 for a function comprising  $K$  input features and one target output, i.e.,  $f: \mathbb{R}^K \rightarrow \mathbb{R}$ . To this end, the neural network  $\text{NN}_{\boldsymbol{\theta}}(\mathbf{x}): \mathbb{R}^K \rightarrow \mathbb{R}$  is trained using the loss

$$r(\boldsymbol{\theta}) = \sum_i \phi \left( f(\mathbf{x}^{(i)}) - \frac{d}{dx_1} \dots \frac{d}{dx_K} \text{NN}(\boldsymbol{\theta}, \mathbf{x}^{(i)}) \right). \quad (16)$$

Then, we can establish the following relation between (i) the trained neural network, (ii) the general anti-derivative (integral) and (iii) the definite anti-derivative (integral) by using the fundamental theorem of calculus (Mutze 2004) according to

$$f(\mathbf{x}) = \frac{d}{dx_1} \dots \frac{d}{dx_K} \text{NN}(\mathbf{x}) \quad (17)$$

$\Updownarrow$

$$\int f(\mathbf{x}) d\mathbf{x} = \text{NN}(\mathbf{x}) \quad (18)$$

$\Updownarrow$

$$\int_{\mathcal{I}} f(\mathbf{x}) d\mathbf{x} = \sum_{\mathbf{x} \in (l_1, u_1) \times \dots \times (l_K, u_K)} (-1)^s \text{NN}(\mathbf{x}), \quad (19)$$

where  $s$  denotes the multiplicity of lower bounds in the evaluated expression.

Using this relation, we can verify that integration over a single variables (e.g.  $x_1$ ) can be obtained for instance in the

3-dimensional case by

$$\int_{l_1}^{u_1} f(x_1, x_2, x_3) dx_1 = \frac{d}{dx_2} \frac{d}{dx_3} \text{NN}(\mathbf{x}) \Big|_{x_1 \in (l_1, u_1)} \quad (20)$$

and integrals over a subset of two variables (e.g.  $x_2, x_3$ ) can be obtained by

$$\int f(x_1, x_2, x_3) dx_2 dx_3 = \frac{d}{dx_1} \text{NN}(\mathbf{x}) \Big|_{x_2, x_3 \in (l_2, u_2) \times (l_3, u_3)}. \quad (21)$$

### Summary of Algorithm

We now present the main result of this paper: a computational algorithm designed to train a neural network, denoted as  $\text{NN}$ , which allows for a closed-form decomposition into lower-dimensional subnetworks  $\text{NN}_{\mathcal{S}}$ . This method is termed *Neural-ANOVA* and summarized in Alg. 2.

In Alg. 2, the following steps are performed in order to calculate the required integrals of the ANOVA decomposition as a signed sum of multiple evaluations of the trained model and the functional transformation of differentiation. First, the model is trained using the loss function specified in (16) where the model is differentiated w.r.t. all input variables. Second, we compute the integral over the subspace spanned by the variables  $\mathbf{x}_{\mathcal{S}^c}$  (cf. (4)) according to

$$\begin{aligned} I_{\mathcal{S}}(\mathbf{x}_{\mathcal{S}}) &= \int_{\mathcal{S}^c} \text{NN}(\mathbf{x}) d\mathbf{x}_{\mathcal{S}^c} = \frac{d^{|\mathcal{S}|}}{d\mathbf{x}_{\mathcal{S}}} \text{NN}(\mathbf{x}) \Big|_{\mathbf{x}_{\mathcal{S}^c} \in (0,1)^{|\mathcal{S}^c|}} \\ &= \sum_{\mathbf{x}_{\mathcal{S}^c} \in (0,1)^{|\mathcal{S}^c|}} \left( (-1)^s \frac{d^{|\mathcal{S}|}}{d\mathbf{x}_{\mathcal{S}}} \text{NN}(\mathbf{x}) \right). \end{aligned} \quad (22)$$

Here, the sign exponent  $s$  denotes the multiplicity of lower bounds in the evaluated expression and  $\mathcal{S}^c := \mathcal{K} \setminus \mathcal{S}$  the complement of  $\mathcal{S}$  over the full index set  $\mathcal{K}$ . In other words, in (22) the trained model is first differentiated w.r.t. the variables in the active-set  $\mathcal{S}$  and then evaluated at the  $2^{|\mathcal{S}^c|}$  corner points of the inactive-set  $\mathcal{S}^c$  that are to be integrated over so that the result is a function of only the variables  $\mathbf{x}_{\mathcal{S}}$ . Lastly, the Neural-ANOVA component  $\text{NN}_{\mathcal{S}}$  is obtained by using the integral calculated in (22) and subtracting the components of all proper subsets

$$\text{NN}_{\mathcal{S}}(\mathbf{x}_{\mathcal{S}}) = \int_{\mathcal{S}^c} \text{NN}(\mathbf{x}) d\mathbf{x}_{\mathcal{S}^c} - \sum_{\mathcal{U} \subset \mathcal{S}} \text{NN}_{\mathcal{U}}(\mathbf{x}_{\mathcal{U}}). \quad (23)$$

The complete resulting algorithm to obtain *Neural-ANOVA* is provided in Alg. 2 where all the neural network terms can be calculated fast and in closed-form at runtime and the variances  $\sigma^2, \sigma_{\mathcal{S}}^2$  can be obtained offline by standard numerical methods such as Monte Carlo approximation.

One approach to calculate the mixed partial derivative in (16) supported by standard automatic differentiation frameworks is to apply nested differentiation. While the implementation of this approach is straight forward e.g. in the automatic differentiation framework JAX (Bradbury et al. 2018), it requires traversing the original computation graph multiple times which may result in redundant computations as was noted in (Hoffmann 2016; Bettencourt, Johnson, and

**Input:** Sampled function  $f(\mathbf{x}) \in \mathcal{L}_2([0, 1]^K)$   
**Output:** Nets  $\{\text{NN}_{\mathcal{S}}\}_{\mathcal{S} \subseteq \mathcal{K}}$ , variances  $\{\sigma_{\mathcal{S}}\}_{\mathcal{S} \subseteq \mathcal{K}}$   
Obtain  $\theta^*$  by training  $f(\mathbf{x}) \approx \frac{d^K}{d\mathbf{x}} \text{NN}_{\theta}(\mathbf{x})$   
 $\text{NN}_{\emptyset} := \sum_{\mathbf{x} \in (0,1)^K} (-1)^s \text{NN}_{\theta}(\mathbf{x})$   
 $\sigma_{\emptyset} := 0$   
**for**  $\mathcal{S} \subseteq \mathcal{K}$ ,  $\mathcal{S} \neq \emptyset$  **do**  
     $\text{NN}_{\mathcal{S}}(\mathbf{x}_{\mathcal{S}}) := \frac{d^{|\mathcal{S}|}}{d\mathbf{x}_{\mathcal{S}}} \text{NN}(\mathbf{x}) \Big|_{\mathbf{x}_{\mathcal{S}^c} \in (0,1)^{K-|\mathcal{S}|}$   
     $-\sum_{\mathcal{U} \subset \mathcal{S}} \text{NN}_{\mathcal{U}}(\mathbf{x}_{\mathcal{U}}) \sigma_{\mathcal{S}}^2 := \int_{[0,1]^{|\mathcal{S}|}} \text{NN}_{\mathcal{S}}^2(\mathbf{x}_{\mathcal{S}}) d\mathbf{x}_{\mathcal{S}}$   
**end**  
 $\sigma^2 := \int_{[0,1]^K} \left(\frac{d^K}{d\mathbf{x}} \text{NN}\right)^2(\mathbf{x}) d\mathbf{x} - \text{NN}_{\emptyset}^2 \equiv \sum_{\mathcal{S} \subseteq \mathcal{K}} \sigma_{\mathcal{S}}^2$

**Algorithm 2:** Neural-ANOVA decomposition of  $f$ , adapted from (Kuo et al. 2010).

Duvenaud 2019). We highlight that also more sophisticated methods for calculating the mixed partial derivative exist compared to the nested approach such as Taylor series approximation, which was shown to admit favorable runtime properties for calculating higher-order derivatives (Betten-court, Johnson, and Duvenaud 2019). In this paper, we chose to retain the nested approach as we observe satisfactory runtime and numerical stability up to moderate dimension  $K \leq 10$ .

### Numerical Example

This section presents a concise numerical example for a common test-function from sensitivity analysis, namely the 3-dimensional *Ishigami*-function

$$f(\mathbf{x}) = \sin(x_1) + a \sin^2(x_2) + b x_3^4 \sin(x_1), \quad (24)$$

with  $a = 7, b = 0.1$ .

We normalize the input and output domain and present the generated data for  $x_3 = 0$  in Fig. 1. The loss function for training the neural network is defined as

$$r(\theta) = \sum_i \left( f(x_1, x_2, x_3) - \frac{d^3}{dx_1 dx_2 dx_3} \text{NN}(x_1, x_2, x_3) \right)^2. \quad (25)$$

Next, we find the terms of the Neural-ANOVA decomposition using the trained network according to

$$\begin{aligned} \text{NN}_{\emptyset} &= \text{NN}(u_1, u_2, u_3) - \text{NN}(u_1, l_2, u_3) \\ &\quad - \text{NN}(l_1, u_2, u_3) + \text{NN}(l_1, l_2, u_3) - \text{NN}(u_1, u_2, l_3) \\ &\quad + \text{NN}(u_1, l_2, l_3) + \text{NN}(l_1, u_2, l_3) - \text{NN}(l_1, l_2, l_3) \end{aligned} \quad (26)$$

$$\text{NN}_1(x_1) = \frac{d}{dx_1} \text{NN}(x_1, x_2, x_3) \Big|_{x_2, x_3 \in (l_2, u_2) \times (l_3, u_3)} - \text{NN}_{\emptyset} \quad (27)$$

$$\begin{aligned} \text{NN}_{1,2}(x_1, x_2) &= \frac{d}{dx_1} \frac{d}{dx_2} \text{NN}(x_1, x_2, x_3) \Big|_{x_3 \in (l_3, u_3)} \\ &\quad - \text{NN}_{\emptyset} - \text{NN}_1(x_1) - \text{NN}_2(x_2) \end{aligned} \quad (28)$$

$\mathcal{S}$	{1}	{2}	{3}	{1, 2}	{1, 3}	{2, 3}
Ref.	0.314	0.442	0.0	0.0	0.244	0.0
Est.	0.305	0.439	6e-9	1e-10	0.256	8e-9

Table 1: True sensitivities and numerical estimates calculated using N-ANOVA for the Ishigami function.

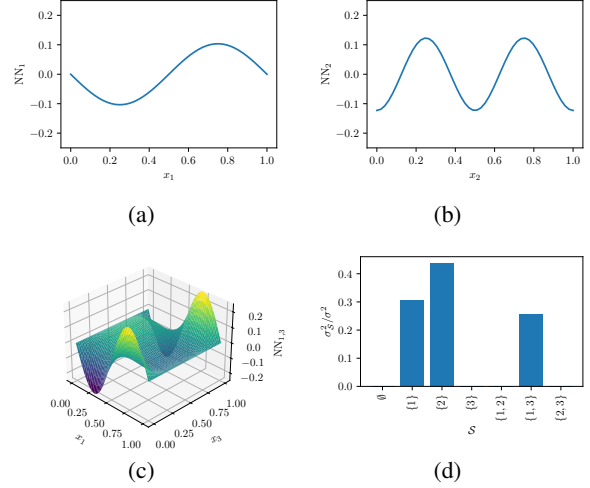


Figure 2: (a-c) Plots of  $\text{NN}_{\mathcal{S}}(\mathbf{x}_{\mathcal{S}})$  for  $\mathcal{S} = \{1\}, \{2\}, \{1, 3\}$ , and (d) sensitivities  $\sigma_{\mathcal{S}}$  for the Ishigami function.

Finally, we can evaluate and illustrate the decomposed function (cf. Fig. 2) and obtain sensitivities using a Monte Carlo estimate according to Alg. 2. We see in Tab. 1 that the sensitivities match well with their closed form expressions (Sobol and Levitan 1999).

### Experiments

This section presents the results of numerical experiments performed on simulation functions from the field of sensitivity analysis and real-world industrial applications.

For sensitivity analysis, we use sampled data of the simulation functions *Ishigami*, *OTL Circuit* and *Piston* from the *UQTestFuns*-library (Wicaksono and Hecht 2023). The training, validation and testing data is generated by evaluating the function using the default sampling distributions and min-max scaling of input and output domain to  $[0, 1]$ . The primary objective of these experiments is to evaluate the expressive power and generalization capabilities of mixed partial derivative networks with different activation functions. The study also examines function properties such as superposition and truncation dimensions.

As industrial datasets we consider Airfoil Self-Noise (ASN), Combined Cycle Power Plant (CCP) and Concrete Compressive Strength (CCS) datasets (Asuncion, Newman et al. 2007). We provide an overview of the considered datasets in Tab. 2. In all cases the data is split into 60/20/20 ratio for training, validation, and, testing, respectively.

We use JAX (Bradbury et al. 2018) to implement both Neural-ANOVA and an MLP baseline. The MLP

serves as benchmark for evaluating the expressive power and noise robustness of different architectures. We experiment with the following standard architectures: (i) 3 layers with 32 neurons and sigmoid activation, and ablations with (ii)  $\{8, 16, 32, 48\}$  hidden neurons and  $\{\text{sigmoid}, \text{relu}, \text{swish}, \text{rep}\}$  activation where rep denotes the rectified polynomial function. The default architecture serves as the model for mixed partial derivative training in the N-ANOVA approach (16) for the simulation functions ISH, CIR and PST and the MLP approach on all datasets. For the ASN, CCP, and CCS datasets, we observe, similar to (Agarwal et al. 2021), the necessity of regularization due to the limited number of data points. For N-ANOVA, our empirical findings indicate that a two-layer architecture with rep activation, 16 neurons and  $\ell_2$ -weight regularization provides satisfactory results for ASN and CCP, but led to a small number of divergent runs, which were excluded from the analysis. This issue could potentially be mitigated through more advanced hyperparameter tuning or by employing methods based on cloning the trained baseline MLP.

We also report results for Neural Additive Models (NAMs), which consist of three layers with 32 neurons and relu activation, following the JAX implementation<sup>1</sup> to maintain consistency with the experimental setup. In Tab. 3, we present a comparison of training time between N-ANOVA and a standard MLP and compare the model sizes of all three approaches in terms of trainable parameters. This confirms that the N-ANOVA model has an identical parameter count to the MLP and the NAM architecture typically contains more parameters due to the  $K$  independent feature networks. Tab. 4 shows the impact of truncating variables on the Ishigami dataset to analyze the effect of reducing input variables, such as in scenarios with missing values.

In Tab. 5, we report the root MSE (RMSE) and standard error on the test set, based on 10 runs with different random seeds. The trainings utilize validation early stopping and are obtained using the adam and bfgs optimizers. We find that MLP and N-ANOVA $_{\infty}$  (all interactions) as well as NAM and N-ANOVA $_1$  (univariate interactions) perform similarly on the simulation functions. For datasets with a small sample count, NAMs demonstrate slightly superior generalization in the univariate setting. This performance can be matched by N-ANOVA $_2$  where bivariate interactions are included. However, N-ANOVA shows performance deterioration for small sample sizes, specifically for 1030 samples in the largest dimension  $K = 8$  of the CCS dataset. These results suggest the potential for developing mixed partial derivative architectures that generalize better in future research.

For the Airfoil dataset, we also depict the shape functions of the N-ANOVA approach and the estimated sensitivities in Fig. 3 where we see that the model assigns a strong impact to a small number of interactions.

Finally, Fig. 4 illustrates ablation studies on the stability of different models and under varying levels of additive noise. The results indicate that the mixed partial derivative networks within the N-ANOVA framework exhibit similar scaling and robustness behavior to a standard MLP archi-

ture where the error level is slightly higher for the N-ANOVA networks. Notably, N-ANOVA models utilizing the relu activation function demonstrate a significant loss in expressive power when subjected to differentiation and the rep activation shows promising robustness to higher noise levels.

Dataset	features	samples
Ishigami (ISH)	3	10000
OTL Circuit (CIR)	6	10000
Piston (PST)	7	10000
Airfoil Self-Noise (ASN)	5	1503
Combined Cycle Power Plant (CCP)	4	9568
Concrete Compressive Strength (CCS)	8	1030

Table 2: Dataset overview.

	MLP	N-ANOVA	NAM
training time	121.3	857.6	—*
parameters	1345	1345	11544

Table 3: Comparison of avg. training time in seconds and number of trainable parameters for the Piston dataset. (\* excluded due to different training framework)

$\mathcal{T}$	$\{1\}$	$\{2\}$	$\{3\}$	$\{1,2\}$	$\{1,3\}$	$\{2,3\}$
N-ANOVA $\setminus\mathcal{T}$	0.09	0.14	0.05	0.17	0.09	0.15
MLP $\setminus\mathcal{T}$	0.09	0.24	0.06	0.26	0.09	0.25

Table 4: Comparison of truncating variables for N-ANOVA using truncated sum (9) and MLP using replacement by mean on Ishigami dataset (RMSE over 10 seeds).

## Conclusion

In this paper, we present an efficient method for computing the functional ANOVA decomposition using neural networks to quantify learned interaction effects across multiple datasets. We derive a novel learning problem focused on computing integrals over subspaces essential to the ANOVA decomposition and demonstrate how this algorithm can decompose a network by fitting the mixed partial derivative to the training data. Our approach is empirically validated on various test functions from uncertainty quantification and real-world industrial datasets, confirming the accuracy of the functional decomposition. We also show that the Neural ANOVA approach can specialize to obtain a generalized additive model. The method provides a principled way to analyze interaction effects, offering deeper insights into training results and the implications of using a specific trained model, allowing domain experts to certify particular use cases. Further research may address more tailored architectures that maintain higher expressive power or generalization under differentiation. Our implementation will be made available with the paper.

<sup>1</sup>[https://github.com/Habush/nam\\_jax](https://github.com/Habush/nam_jax)

	MLP	N-ANOVA <sub>∞</sub>	N-ANOVA <sub>4</sub>	N-ANOVA <sub>3</sub>	N-ANOVA <sub>2</sub>	N-ANOVA <sub>1</sub>	NAM
ISH	1.7E-04 ±0.5E-04	1.2E-04 ±0.2E-04	1.2E-04 ±0.2E-04	1.2E-04 ±0.2E-04	1.2E-04 ±0.2E-04	<b>5.06E-02</b> ±0.04E-02	<b>5.08E-02</b> ±0.05E-02
CIR	5.8E-05 ±1.5E-05	1.3E-04 ±0.3E-04	1.1E-04 ±0.2E-04	1.0E-04 ±0.2E-04	1.1E-04 ±0.2E-04	<b>1.59E-02</b> ±0.01E-02	<b>1.61E-02</b> ±0.02E-02
PST	5.2E-05 ±0.8E-05	1.65E-04 ±0.2E-04	2.52E-04 ±0.07E-04	2.96E-03 ±0.05E-03	1.62E-02 ±0.03E-02	<b>3.94E-02</b> ±0.04E-02	<b>3.86E-02</b> ±0.06E-02
ASN	4.4E-02 ±0.2E-02	9.0E-02 ±0.3E-02	9.0E-02 ±0.3E-02	1.00E-01 ±0.09E-01	<b>1.19E-01</b> ±0.07E-01	1.67E-01 ±0.07E-01	<b>1.23E-01</b> ±0.02E-01
CCP	5.33E-02 ±0.08E-02	5.73E-02 ±0.05E-02	5.73E-02 ±0.05E-02	5.74E-02 ±0.05E-02	<b>5.77E-02</b> ±0.05E-02	5.95E-02 ±0.06E-02	<b>5.68E-02</b> ±0.06E-02
CCS	7.4E-02 ±0.2E-02	1.03E-01 ±0.06E-01	1.03E-01 ±0.06E-01	1.04E-01 ±0.06E-01	1.06E-01 ±0.06E-01	1.51E-01 ±0.2E-01	<b>7.1E-02</b> ±0.2E-02

Table 5: Performance comparison of proposed N-ANOVA<sub>d<sub>s</sub></sub> with varying superposition dimension d<sub>s</sub>, Neural Additive Model (NAM) (Agarwal et al. 2021) (i.e., d<sub>s</sub> = 1) and Multi-Layer Perceptron (MLP) (d<sub>s</sub> = K). The error is shown as RMSE on holdout set (lower is better).

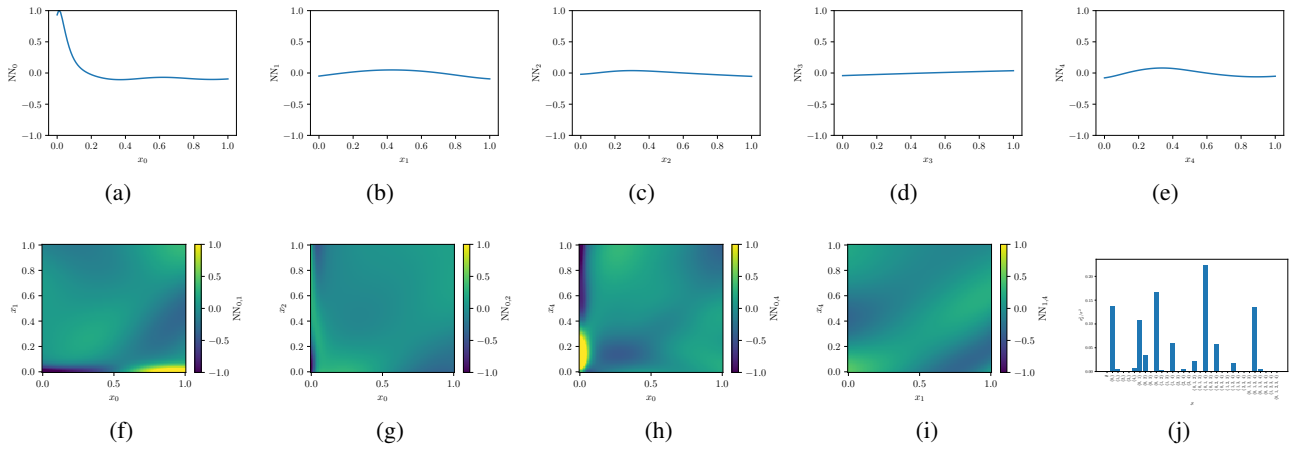


Figure 3: Plots of (a)-(e)  $NN_k(\mathbf{x}_k)$ , (f)-(i)  $NN_S(\mathbf{x}_S)$ , (j) sensitivities  $\sigma_S$  for the Airfoil dataset.

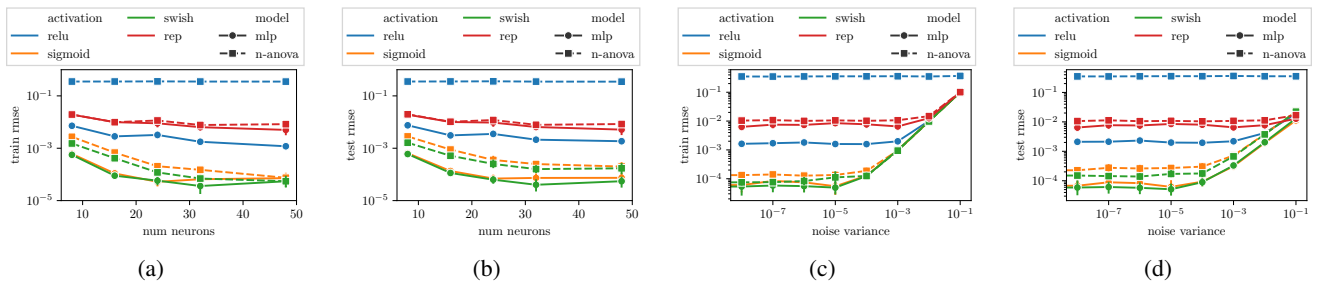


Figure 4: Ablation on (a)-(b) training and testing error for varying number of hidden layer neurons and (c)-(d) for varying level of additive training noise and varying activation functions on the Piston dataset.

## References

- Adachi, M.; Kuhn, Y.; Horstmann, B.; Latz, A.; Osborne, M. A.; and Howey, D. A. 2023. Bayesian model selection of lithium-ion battery models via Bayesian quadrature. *IFAC-PapersOnLine*, 56(2): 10521–10526.
- Agarwal, R.; Melnick, L.; Frosst, N.; Zhang, X.; Lengerich, B.; Caruana, R.; and Hinton, G. E. 2021. Neural additive models: interpretable machine learning with neural nets. In *Proceedings of the 35th International Conference on Neural Information Processing Systems*.
- Asuncion, A.; Newman, D.; et al. 2007. UCI machine learning repository.
- Berg, D. 2007. Bankruptcy prediction by generalized additive models. *Applied Stochastic Models in Business and Industry*, 23(2): 129–143.
- Bettencourt, J.; Johnson, M. J.; and Duvenaud, D. 2019. Taylor-mode automatic differentiation for higher-order derivatives in JAX. In *Program Transformations for ML Workshop at NeurIPS 2019*.
- Bradbury, J.; Frostig, R.; Hawkins, P.; Johnson, M. J.; Leary, C.; Maclaurin, D.; Necula, G.; Paszke, A.; VanderPlas, J.; Wanderman-Milne, S.; and Zhang, Q. 2018. JAX: composable transformations of Python+NumPy programs.
- Breiman, L.; and Friedman, J. H. 1985. Estimating optimal transformations for multiple regression and correlation. *Journal of the American statistical Association*, 80(391): 580–598.
- Gao, K.; Gao, Y.; He, H.; Lu, D.; Xu, L.; and Li, J. 2022. NeRF: Neural radiance field in 3D vision, a comprehensive review. *arXiv preprint arXiv:2210.00379*.
- Hastie, T. J. 2017. Generalized additive models. In *Statistical models in S*, 249–307. Routledge.
- Hegselmann, S.; Volkert, T.; Ohlenburg, H.; Gottschalk, A.; Dugas, M.; and Ertmer, C. 2020. An evaluation of the doctor-interpretability of generalized additive models with interactions. In *Machine Learning for Healthcare Conference*, 46–79. PMLR.
- Hoeffding, W.; and Robbins, H. 1948. The central limit theorem for dependent random variables. *Duke Mathematical Journal*, 15(3): 773.
- Hoffmann, P. H. 2016. A hitchhiker’s guide to automatic differentiation. *Numerical Algorithms*, 72(3): 775–811.
- Hooker, G. 2004. Discovering additive structure in black box functions. In *Proceedings of the tenth ACM SIGKDD international conference on Knowledge discovery and data mining*, 575–580.
- Hutter, F.; Hoos, H.; and Leyton-Brown, K. 2014. An efficient approach for assessing hyperparameter importance. In *International conference on machine learning*, 754–762. PMLR.
- Kuo, F.; Sloan, I.; Wasilkowski, G.; and Woźniakowski, H. 2010. On decompositions of multivariate functions. *Mathematics of computation*, 79(270): 953–966.
- Limmer, S.; Alba, A. M.; and Michailow, N. 2023. Physics-informed neural networks for pathloss prediction. In *2023 IEEE 33rd International Workshop on Machine Learning for Signal Processing (MLSP)*, 1–5. IEEE.
- Lindell, D.; Martel, J.; and Wetzstein, G. 2021. Autoint: Automatic integration for fast neural volume rendering. In *Proceedings of the IEEE/CVF Conference on Computer Vision and Pattern Recognition*, 14556–14565.
- Mutze, U. 2004. The Fundamental Theorem of Calculus in  $\mathbb{R}^n$ . Technical report, University of Texas.
- Owen, A. 2023. Practical Quasi-Monte Carlo. *Draft available at <https://artowen.su.domains/mc/practicalqmc.pdf>*. Accessed 14th August.
- Potts, D.; and Schmischke, M. 2021. Interpretable approximation of high-dimensional data. *SIAM Journal on Mathematics of Data Science*, 3(4): 1301–1323.
- Risch, R. H. 1969. The problem of integration in finite terms. *Transactions of the American Mathematical Society*, 139: 167–189.
- Rückert, D.; Wang, Y.; Li, R.; Idoughi, R.; and Heidrich, W. 2022. Neat: Neural adaptive tomography. *ACM Transactions on Graphics (TOG)*, 41(4): 1–13.
- Sobol, I. M. 2001. Global sensitivity indices for nonlinear mathematical models and their Monte Carlo estimates. *Mathematics and computers in simulation*, 55(1-3): 271–280.
- Sobol, I. M.; and Levitan, Y. L. 1999. On the use of variance reducing multipliers in Monte Carlo computations of a global sensitivity index. *Computer Physics Communications*, 117(1): 52–61.
- Wahba, G. 1990. *Spline Models for Observational Data*. CBMS-NSF Regional Conference Series in Applied Mathematics. Society for Industrial and Applied Mathematics. ISBN 9780898712445.
- Wicaksono, D.; and Hecht, M. 2023. UQTestFuns: A Python3 library of uncertainty quantification (UQ) test functions. *Journal of Open Source Software*, 8(90): 5671.
- Yang, X.; Choi, M.; Lin, G.; and Karniadakis, G. E. 2012. Adaptive ANOVA decomposition of stochastic incompressible and compressible flows. *Journal of Computational Physics*, 231(4): 1587–1614.
- Zhou, Z.; and Yu, R. 2024. Automatic integration for spatiotemporal neural point processes. *Advances in Neural Information Processing Systems*, 36.